

Performance of Intelligent Reconfigurable Surface-Based Wireless Communications Using QAM Signaling

Dharmendra Dixit , Kishor Chandra Joshi , Sanjeev Sharma ,

Abstract

Intelligent reconfigurable surface (IRS) is being seen as a promising technology for 6G wireless networks. The IRS can reconfigure the wireless propagation environment, which results in significant performance improvement of wireless communications. In this paper, we analyze the performance of bandwidth-efficient quadrature amplitude modulation (QAM) techniques for IRS-assisted wireless communications over Rayleigh fading channels. New closed-form expressions of the generic average symbol error rate (ASER) for rectangular QAM, square QAM and cross QAM schemes are derived. Moreover, simplified expressions of the ASER for low signal-to-noise-ratio (SNR) and high SNR regions are also presented, which are useful to provide insights analytically. We comprehensively analyze the impact of modulation parameters and the number of IRS elements employed. We also verify our theoretical results through simulations. Our results demonstrate that employing IRS significantly enhances the ASER performance in comparison to additive white Gaussian noise channel at a low SNR regime. Thus, IRS-assisted wireless communications can be a promising candidate for various low powered communication applications such as internet-of-things (IoT).

Index Terms

Wireless communications, Intelligent reconfigurable surface (IRS), Rayleigh fading, Quadrature amplitude modulation (QAM).

I. INTRODUCTION

In recent years, unprecedented growth of mobile data traffic is witnessed due to the rapid proliferation of various wireless communication technologies, applications, and services. In general, 5G standardization goals are defined based on enhanced mobile broadband, ultra-reliable and low latency communications and massive machine-type communications to address the key wireless communication requirements. To fulfill the above requirements, different techniques such as Millimeter-wave (mmWave) communication, massive multiple-input multiple-output (MIMO), new waveform design, ultra-dense network (UDN), etc. are proposed [1]. Further, spectral and energy efficient wireless systems design is a key requirement for 5G and beyond wireless networks, and recently proposed intelligent reconfigurable surface (IRS)-assisted wireless system design can improve spectral and energy efficiency significantly by enhancing the received signal power at a user node [2].

One common feature of all the previous generations of wireless communications up to 5G is the assumption that wireless channel is truly random and hence cannot be controlled. Thus the various mechanisms (e.g., MIMO, orthogonal frequency-division multiplexing (OFDM), etc.) developed for the performance improvement of wireless communication systems over the years considered wireless channel impairments as unavoidable and tried to mitigate the adverse effects of wireless channel at the transmitter and receiver. Recently, a new technique called the IRS, which uses artificial materials to control the propagation characteristics of the radio environment, is being seen a revolutionary technology to enhance the performance of future wireless systems [2–4]. Instead of compensating the destructive effects of

propagation environment at receiver and transmitter, IRS allows the radio environments to reconfigure itself in such a way that the negative effects of the environment are undone before it reaches the receiver. The ability to control wireless channel brings a true paradigm shift in the fundamentals of design and deployment of wireless communication systems since the interaction of radio signal with the radio environment can be deterministically defined to a large extent.

The key underline principle of the IRS-assisted communications is to tune the radio environment (obstacles, reflectors, etc.) such that the resulting end-to-end communication channel is favorable to radio signal transmission [5]. IRSs are artificial surfaces whose electromagnetic response can be electronically controllable. This allows IRS elements to reflect/refract signals at any desired angle. It becomes specifically beneficial in the context of upcoming 5G and 6G systems employing mmWave and Terahertz bands [6, 7] where providing ubiquitous coverage is very difficult due to a high signal absorption by obstacles/wireless environment. IRSs are also important from the energy efficiency perspective as the IRSs do not involve any encoding/decoding or amplification of impinged signal while significantly improving the signal power at the intended receiver [8].

Recently, research on IRS-assisted communications has received tremendous attention for wireless communications due to its potential applications in improving the coverage, energy-efficiency and data-rates. In the seminal work on IRS [9], a mathematical model for IRS-assisted communication is presented. The extension of the proposed model by employing beamforming-based design to model the IRS is presented [10]. In [11], a detailed physical channel model considering the physical dimensions of IRS, element spacing, and radiation pattern is proposed and the relation between the size of IRS and path-loss is numerically established. In [12], the impacts of overheads resulting due to feedback on the spectral efficiency are analyzed. In [13], authors investigate theoretical performance limits of IRS-assisted communication systems using a binary modulation scheme. In [14], a modeling framework for IRS-assisted communications using stochastic geometry is proposed. Performance comparison considering reflection probability defined as the availability of reflected path between transmitter and receiver with and without the IRS-coated obstacles is provided. Similarly, using the stochastic geometry approach, the application of IRS to mitigate the coverage holes in dense-urban environments is explored in [15]. In [16], authors develop closed-form expression for reflected power from IRS using the general scalar theory of diffraction and the Hygens-Fresnel principle as a function of the transmitter/receiver and IRS distance, phase-transformation applied by IRS and the size of IRS. The proposed approach identify the conditions in which IRS behaves as an anomalous reflector resulting in the path loss proportional to the summation of distances between the transmitter-IRS and IRS-receiver. In [17], IRS-assisted communication is compared with the decode-and-forward relaying and relationship between the size of IRS and corresponding performance gain is derived. The N^2 power scaling law of IRS is revisited in [18] and it is shown that with an increasing number of IRS elements, when the far-field assumption is no longer valid, power scaling does not change by the N^2 factor, where N denotes the total number of elements in the IRS.

Quadrature amplitude modulation (QAM) is a generic modulation scheme, which several well-known modulation scheme as special cases. Rectangular QAM (RQAM), square QAM (SQAM) and cross QAM (XQAM) are three main types of QAM schemes. Employing QAM has become an essential practice in modern wireless systems due to the high spectral-efficiency offered by QAMs. For example, 3GPP Release-14 (LTE-advanced) and Release-15 (5G-New radio) specifications already support up to 256-QAMs. Since IRSs can significantly improve the signal strength without introducing any additional noise, the usage of higher order QAMs would be highly beneficial to enhance the spectral efficiency.

To the best of our knowledge, there is no work in the literature on the the performance of QAM signaling for IRS-assisted wireless communications. Motivated by applicability and importance of the aforementioned problem, a comprehensive analytical performance analysis of IRS-assisted wireless communications using QAM signals are given. In this paper, new closed-form analytical expressions for the generic average symbol error rate (ASER) of IRS-assisted wireless communications employing RQAM and XQAM signaling are derived. Moreover, simplified expressions for both low signal-to-noise-ratio (SNR) and high SNR values are also obtained. We comprehensively analyze the different trade-offs resulting

due to modulation parameters and the number of IRS elements employed. We also verify our theoretical results through simulations.

The remaining of this paper is structured as follows. Section II presents system and channel models followed by derivations of closed form expressions in Section III. In Section IV, numerical results and discussion are presented. The conclusion of paper is given in Section V.

II. SYSTEM AND CHANNEL MODELS

The system model consists of a source node (S) and a destination node (D) assisted by a N -element IRS as shown in Fig. 1. We assume that both S and D have a single antenna. The function of each

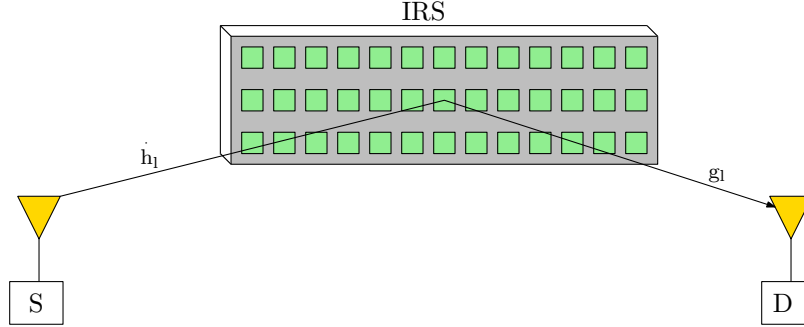


Fig. 1: IRS-assisted dual-hop communication system without a line-of-sight path between source S and destination D .

IRS element is to introduce desired phase-shift to incident signal. h_l and g_l represent the fading channel coefficients between the S and the l -th element of IRS, and between the l -th element of IRS and the D , respectively ($l = 1, 2, \dots, N$). Under the assumption of Rayleigh fading channels, h_l and g_l can be modeled as complex Gaussian distribution with zero mean and unity variance. We assume that the S transmits symbol x with average energy E_s . Therefore, the received signal at the D for a slowly varying and flat fading conditions can be written as

$$r = \mathbf{g}^T \mathbf{\Psi} \mathbf{h} x + n, \quad (1)$$

where $\mathbf{h} = [|h_1| \exp(-j\psi_1), |h_2| \exp(-j\psi_2), \dots, |h_N| \exp(-j\psi_N)]^T$ and $\mathbf{g} = [|g_1| \exp(-j\phi_1), |g_2| \exp(-j\phi_2), \dots, |g_N| \exp(-j\phi_N)]^T$ represent the vectors of fading coefficients between the S and the IRS, and between the D and the IRS, respectively, and $\mathbf{\Psi} = \text{diag}([\exp(-j\varphi_1), \exp(-j\varphi_2), \dots])$ is a diagonal matrix that contains the phase shifts introduced by the N -element IRS. n denotes the additive white Gaussian noise (AWGN) sample modeled as complex Gaussian distribution with zero mean and N_0 variance. Assuming the perfect knowledge of channel coefficients h_l and g_l at IRS, the instantaneous SNR at D can be expressed as follows

$$\gamma = \left(\sum_{l=1}^N |h_l| |g_l| \right)^2 \frac{E_s}{N_0}. \quad (2)$$

Since $|h_l|$ and $|g_l|$ are assumed to be independently Rayleigh distributed random variables (RVs), the mean value and the variance of their product are $\mathbf{E}[|h_l| |g_l|] = 0.25\pi$ and $\mathbf{Var}[|h_l| |g_l|] = 1 - 0.0625\pi^2$, respectively, where $\mathbf{E}[\cdot]$ is an expectation operator and $\mathbf{Var}[|h_l| |g_l|]$ is a variance operator. For a sufficiently large value of N i.e., $N \gg 1$, according to the central limit theorem, $\sum_{l=1}^N |h_l| |g_l|$ converges to a Gaussian distributed RV with statistical parameters $\mathbf{E}\left[\sum_{l=1}^N |h_l| |g_l|\right] = 0.25\pi N$ and $\mathbf{Var}\left[\sum_{l=1}^N |h_l| |g_l|\right] =$

$(1 - 0.0625\pi^2)N$. Hence, the RV γ is a non-central chi-square RV with one degree of freedom and has the following moment generating function (MGF) $\mathcal{G}_\gamma(s)$ [13, 19]

$$\mathcal{G}_\gamma(s) \approx \left(\frac{\Delta_1}{\Delta_1 + s\bar{\gamma}} \right)^{0.5} \exp \left(-\frac{s\bar{\gamma}\Delta_2}{\Delta_1 + s\bar{\gamma}} \right), \quad (3)$$

where $\Delta_1 = \frac{8}{N(16-\pi^2)}$, $\Delta_2 = \frac{N\pi^2}{2(16-\pi^2)}$, and $\bar{\gamma} = \frac{E_s}{N_0}$.

III. PERFORMANCE ANALYSIS

ASER is defined as the averaging of conditional symbol error rate (SER) $P_{e|\gamma}(\cdot)$ over the PDF $f_\gamma(\cdot)$ of SNR γ [20], i.e.,

$$P_e = \mathbb{E} [P_{e|\gamma}(x)] = \int_0^\infty P_{e|\gamma}(x) f_\gamma(x) dx. \quad (4)$$

A. M -ary Rectangular QAM

The expression of conditional SER $P_{e|\gamma}(x)$ for M -ary RQAM is given as [21]

$$P_{e|\gamma}(x) = 2p Q(a\sqrt{x}) + 2q Q(b\sqrt{x}) - 4pq Q(a\sqrt{x}) Q(b\sqrt{x}), \quad (5)$$

where $M = M_I \times M_Q$, $p = 1 - \frac{1}{M_I}$, $q = 1 - \frac{1}{M_Q}$, $a = \sqrt{\frac{6}{(M_I^2-1)+(M_Q^2-1)\beta^2}}$, $b = \beta a$ and $\beta = d_Q/d_I$ is the quadrature-to-in-phase decision distance ratio with d_I and d_Q being the in-phase and quadrature decision distance, respectively and $Q(t)$ is the Gaussian Q -function defined by $Q(t) = \frac{1}{\sqrt{2\pi}} \int_t^\infty \exp(-\frac{x^2}{2}) dx$. For the convenience of analysis, (5) can be rewritten using an alternate expression of 1- D and 2- D Gaussian Q -functions, $Q_z(t, \phi)$ defined as [20]

$$Q_z(t, \theta) = \frac{1}{\pi} \int_0^\theta \exp\left(-\frac{t^2}{2\sin^2\phi}\right) d\phi, \quad t \geq 0. \quad (6)$$

With the aid of (6), it can be obtained that the $Q(t) = Q_z(t, \pi/2)$ [20, (4.2)] and $Q(t)Q(u) = 0.5[Q_z(u, \arctan(u/t))Q_z(t, \operatorname{arccot}(u/t))]$ [20, (4.8)] for $t \geq 0, u \geq 0$. Thus, employing (6), (5) has been expressed as

$$P_{e|\gamma}(x) = 2p Q_z(a\sqrt{x}, \pi/2) + 2q Q_z(b\sqrt{x}, \pi/2) - 2pq \left[Q_z(b\sqrt{x}, \arctan(b/a)) + Q_z(a\sqrt{x}, \operatorname{arccot}(b/a)) \right]. \quad (7)$$

Substituting (7) into (4) and by doing a few simplifications, ASER for RQAM scheme denoted as P_e^{RQAM} , can be written as

$$P_e^{\text{RQAM}} = 2p \mathcal{I}(a, \pi/2) + 2q \mathcal{I}(b, \pi/2) - 2pq \left[\mathcal{I}(b, \arctan(b/a)) + \mathcal{I}(a, \operatorname{arccot}(b/a)) \right], \quad (8)$$

where the integral $\mathcal{I}(\cdot, \cdot)$ is expressed as

$$\begin{aligned} \mathcal{I}(c, \theta) &= \int_0^\infty Q_z(c\sqrt{x}, \theta) f_\gamma(x) dx \\ &= \frac{1}{\pi} \int_0^\theta \int_0^\infty \exp\left(-\frac{c^2 x}{2\sin^2\phi}\right) f_\gamma(x) dx d\phi \\ &= \frac{1}{\pi} \int_0^\theta \mathcal{G}_\gamma\left(\frac{c^2}{2\sin^2\phi}\right) d\phi. \end{aligned} \quad (9)$$

Here $\mathcal{G}_\gamma(\cdot)$ is the MGF of γ . Thus, to obtain a solution of (9), we need the MGF of γ which is given in (3). Substituting (3) in (9), closed-form solutions for $\mathcal{I}(x, \pi/2)$, $\mathcal{I}(b, \arctan(b/a))$ and $\mathcal{I}(x, \operatorname{arccot}(b/a))$, which will be employed to compute (8), are obtained in (32), (33) and (34), respectively, in Appendix A.

$$\begin{aligned}
P_e^{\text{RQAM}} \approx & \frac{2pa\sqrt{2\Delta_1\bar{\gamma}} \exp(-\Delta_2)}{\pi(a^2\bar{\gamma} + 2\Delta_1)} \Phi_1^{(2)} \left(1; 1; 1.5; \frac{2\Delta_1}{a^2\bar{\gamma} + 2\Delta_1}, \frac{2\Delta_1\Delta_2}{a^2\bar{\gamma} + 2\Delta_1} \right) \\
& + \frac{2qb\sqrt{2\Delta_1\bar{\gamma}} \exp(-\Delta_2)}{\pi(b^2\bar{\gamma} + 2\Delta_1)} \Phi_1^{(2)} \left(1; 1; 1.5; \frac{2\Delta_1}{b^2\bar{\gamma} + 2\Delta_1}, \frac{2\Delta_1\Delta_2}{b^2\bar{\gamma} + 2\Delta_1} \right) \\
& - \frac{2pqb\sqrt{2\Delta_1\bar{\gamma}} \exp(-\Delta_2)}{2\pi((a^2 + b^2)\bar{\gamma} + 2\Delta_1)} \Phi_1^{(3)} \left(1; 0.5, 1; 2; \frac{(b^2\bar{\gamma} + 2\Delta_1)}{(a^2 + b^2)\bar{\gamma} + 2\Delta_1}, \right. \\
& \left. \frac{2\Delta_1}{(a^2 + b^2)\bar{\gamma} + 2\Delta_1}, \frac{2\Delta_1\Delta_2}{(a^2 + b^2)\bar{\gamma} + 2\Delta_1} \right) - \frac{2pqa\sqrt{2\Delta_1\bar{\gamma}} \exp(-\Delta_2)}{2\pi((a^2 + b^2)\bar{\gamma} + 2\Delta_1)} \\
& \times \Phi_1^{(3)} \left(1; 0.5, 1; 2; \frac{a^2\bar{\gamma} + 2\Delta_1}{(a^2 + b^2)\bar{\gamma} + 2\Delta_1}, \frac{2\Delta_1}{(a^2 + b^2)\bar{\gamma} + 2\Delta_1}, \frac{2\Delta_1\Delta_2}{(a^2 + b^2)\bar{\gamma} + 2\Delta_1} \right). \quad (10)
\end{aligned}$$

$$\begin{aligned}
P_e^{\text{SQAM}} \approx & \frac{4\tilde{p}\tilde{a}\sqrt{2\Delta_1\bar{\gamma}} \exp(-\Delta_2)}{\pi(\tilde{a}^2\bar{\gamma} + 2\Delta_1)} \Phi_1^{(2)} \left(1; 1; 1.5; \frac{2\Delta_1}{\tilde{a}^2\bar{\gamma} + 2\Delta_1}, \frac{2\Delta_1\Delta_2}{\tilde{a}^2\bar{\gamma} + 2\Delta_1} \right) \\
& - \frac{\tilde{p}^2\tilde{a}\sqrt{2\Delta_1\bar{\gamma}} \exp(-\Delta_2)}{\pi(\tilde{a}^2\bar{\gamma} + \Delta_1)} \Phi_1^{(3)} \left(1; 0.5, 1; 2; \frac{(\tilde{a}^2\bar{\gamma} + 2\Delta_1)}{2\tilde{a}^2\bar{\gamma} + 2\Delta_1}, \frac{\Delta_1}{\tilde{a}^2\bar{\gamma} + \Delta_1}, \frac{\Delta_1\Delta_2}{\tilde{a}^2\bar{\gamma} + \Delta_1} \right) \quad (11)
\end{aligned}$$

$$P_e^{\text{BPSK}} \approx \frac{\sqrt{\Delta_1\bar{\gamma}} \exp(-\Delta_2)}{\pi(\bar{\gamma} + \Delta_1)} \Phi_1^{(2)} \left(1; 1; 1.5; \frac{\Delta_1}{\bar{\gamma} + \Delta_1}, \frac{\Delta_1\Delta_2}{\bar{\gamma} + \Delta_1} \right). \quad (12)$$

Thus, substituting these solutions in (8) and simplifying the resulting expression, an ASER expression for P_e^{RQAM} can be obtained as in (10). For the special case of M -ary SQAM, i.e. when $M_I = M_Q = \sqrt{M}$ and $\beta = 1$, one can get ASER expression of M -ary SQAM which is provided in (11), where $\tilde{p} = 1 - \frac{1}{\sqrt{M}}$ and $\tilde{a} = \sqrt{\frac{3}{M-1}}$. Similarly, for BPSK, i.e. when $M_I = 2$, $M_Q = 1$ and $\beta = 0$, one can obtain ASER expression of BPSK which is given in (12). It is important to mention that (11) and (12) are the closed-form solutions of [13, (21)] and [13, (17)], respectively.

B. M -ary Cross QAM

The conditional SER $P_{e|\gamma}(x)$ for M -ary XQAM can be given as [22]

$$\begin{aligned}
P_{e|\gamma}(x) = & w_1 Q_z(a_0\sqrt{x}, \pi/2) + w_2 Q_z(a_1\sqrt{x}, \pi/2) - w_3 Q_z(a_0\sqrt{x}, \pi/4) \\
& - 2w_2 \sum_{l=1}^{L-1} Q_z(a_0\sqrt{x}, \alpha_l) - w_2 \sum_{l=1}^{L-1} Q_z(a_l\sqrt{x}, \beta_l^+) + w_2 \sum_{l=2}^L Q_z(a_l\sqrt{x}, \beta_l^-), \quad (13)
\end{aligned}$$

where $w_1 = 4 - \frac{6}{\sqrt{2M}}$, $w_2 = \frac{4}{M}$, $w_3 = 4 - \frac{12}{\sqrt{2M}} + \frac{12}{M}$, $L = \frac{\sqrt{2M}}{8}$, $a_0 = \sqrt{\frac{96}{(31M-32)}}$, $a_l = \sqrt{2}la_0$, $l = 1, 2, \dots, L$, $\alpha_l = \arctan\left(\frac{1}{2l+1}\right)$, $l = 1, 2, \dots, (L-1)$; $\beta_l^- = \arctan\left(\frac{l}{l-1}\right)$, $l = 2, 3, \dots, L$; $\beta_l^+ = \arctan\left(\frac{l}{l+1}\right)$, $l = 1, 2, \dots, L-1$.

$$\begin{aligned}
P_e^{\text{XQAM}} \approx & \frac{w_1 a_0 \sqrt{2\Delta_1 \bar{\gamma}} \exp(-\Delta_2)}{\pi(a_0^2 \bar{\gamma} + 2\Delta_1)} \Phi_1^{(2)} \left(1; 1; 1.5; \frac{2\Delta_1}{a_0^2 \bar{\gamma} + 2\Delta_1}, \frac{2\Delta_1 \Delta_2}{a_0^2 \bar{\gamma} + 2\Delta_1} \right) \\
& + \frac{w_2 a_1 \sqrt{2\Delta_1 \bar{\gamma}} \exp(-\Delta_2)}{\pi(a_1^2 \bar{\gamma} + 2\Delta_1)} \Phi_1^{(2)} \left(1; 1; 1.5; \frac{2\Delta_1}{a_1^2 \bar{\gamma} + 2\Delta_1}, \frac{2\Delta_1 \Delta_2}{a_1^2 \bar{\gamma} + 2\Delta_1} \right) \\
& - \frac{w_3 a_0 \sqrt{2\Delta_1 \bar{\gamma}} \exp(-\Delta_2)}{4\pi(a_0^2 \bar{\gamma} + \Delta_1)} \Phi_1^{(3)} \left(1; 0.5, 1; 2; \frac{(a_0^2 \bar{\gamma} + 2\Delta_1)}{2a_0^2 \bar{\gamma} + 2\Delta_1}, \frac{\Delta_1}{a_0^2 \bar{\gamma} + \Delta_1}, \frac{\Delta_1 \Delta_2}{a_0^2 \bar{\gamma} + \Delta_1} \right) \\
& - 2w_2 \sum_{l=1}^{L-1} \frac{a_0 \sqrt{2\Delta_1 \bar{\gamma}} \exp(-\Delta_2)}{2\pi(a_0^2(1 + (2l+1)^2)\bar{\gamma} + 2\Delta_1)} \Phi_1^{(3)} \left(1; 0.5, 1; 2; \frac{(a_0^2 \bar{\gamma} + 2\Delta_1)}{a_0^2(1 + (2l+1)^2)\bar{\gamma} + 2\Delta_1}, \right. \\
& \left. \frac{2\Delta_1}{a_0^2(1 + (2l+1)^2)\bar{\gamma} + 2\Delta_1}, \frac{2\Delta_1 \Delta_2}{a_0^2(1 + (2l+1)^2)\bar{\gamma} + 2\Delta_1} \right) \\
& - w_2 \sum_{l=1}^{L-1} \frac{a_l l^2 \sqrt{2\Delta_1 \bar{\gamma}} \exp(-\Delta_2)}{2\pi(a_l^2(l^2 + (l-1)^2)\bar{\gamma} + 2\Delta_1 l^2)} \Phi_1^{(3)} \left(1; 0.5, 1; 2; \frac{(a_l^2 \bar{\gamma} + 2\Delta_1)l^2}{a_l^2(l^2 + (l-1)^2)\bar{\gamma} + 2\Delta_1 l^2}, \right. \\
& \left. \frac{2\Delta_1 l^2}{a_l^2(l^2 + (l-1)^2)\bar{\gamma} + 2\Delta_1 l^2}, \frac{2\Delta_1 \Delta_2 l^2}{a_l^2(l^2 + (l-1)^2)\bar{\gamma} + 2\Delta_1 l^2} \right) \\
& + w_2 \sum_{l=2}^L \frac{a_l l^2 \sqrt{2\Delta_1 \bar{\gamma}} \exp(-\Delta_2)}{2\pi(a_l^2(l^2 + (l+1)^2)\bar{\gamma} + 2\Delta_1 l^2)} \Phi_1^{(3)} \left(1; 0.5, 1; 2; \frac{(a_l^2 \bar{\gamma} + 2\Delta_1)l^2}{a_l^2(l^2 + (l+1)^2)\bar{\gamma} + 2\Delta_1 l^2}, \right. \\
& \left. \frac{2\Delta_1 l^2}{a_l^2(l^2 + (l+1)^2)\bar{\gamma} + 2\Delta_1 l^2}, \frac{2\Delta_1 \Delta_2 l^2}{a_l^2(l^2 + (l+1)^2)\bar{\gamma} + 2\Delta_1 l^2} \right) \tag{15}
\end{aligned}$$

Substituting (13) into (4) and using (6), the ASER expression of XQAM can be written as

$$\begin{aligned}
P_e^{\text{XQAM}} = & w_1 \mathcal{I}(a_0, \pi/2) + w_2 \mathcal{I}(a_1, \pi/2) - w_3 \mathcal{I}(a_0, \pi/4) - 2w_2 \sum_{l=1}^{L-1} \mathcal{I}(a_0, \alpha_l) \\
& - w_2 \sum_{l=1}^{L-1} \mathcal{I}(a_l, \beta_l^+) + w_2 \sum_{l=2}^L \mathcal{I}(a_l, \beta_l^-), \tag{14}
\end{aligned}$$

where $\mathcal{I}(\cdot, \cdot)$ is given in (9). To obtain a closed-form solution of (14), it is required to obtain the solution of $\mathcal{I}(c, \theta)$. The desired solutions are given in Appendix A. Employing a similar method as followed to obtain (10), an ASER expression of XQAM can be written as (15), at the top of the next page.

C. Low SNR Analysis for IRS

At low SNR region, one can approximate MGF expression in (3) as given below

$$\mathcal{G}_\gamma^L(s) \approx \exp\left(-\frac{\Delta_2}{\Delta_1} s \bar{\gamma}\right), \tag{16}$$

Hence, the ASER expression of RQAM at low SNR region can be expressed as

$$P_{e, \text{low SNR}}^{\text{RQAM}} = 2p \mathcal{I}^L(a, \pi/2) + 2q \mathcal{I}^L(b, \pi/2) - 2pq \left[\mathcal{I}^L(b, \arctan(b/a)) + \mathcal{I}^L(a, \text{arccot}(b/a)) \right], \tag{17}$$

where the integral $\mathcal{I}^L(\cdot, \cdot)$ is given as

$$\mathcal{I}^L(c, \theta) = \frac{1}{\pi} \int_0^\theta \mathcal{G}_\gamma^L \left(\frac{c^2}{2 \sin^2 \phi} \right) d\phi, \quad (18)$$

In order to get insights, (18) can be upper bounded by setting $\phi = \theta$, which gives

$$\begin{aligned} \mathcal{I}^L(c, \theta) &\leq \frac{\theta}{\pi} \mathcal{G}_\gamma^L \left(\frac{c^2}{2 \sin^2 \theta} \right) \\ &\leq \frac{\theta}{\pi} \exp \left(-\frac{\Delta_2 c^2 \bar{\gamma}}{2 \Delta_1 \sin^2 \theta} \right) \\ &\leq \frac{\theta}{\pi} \exp \left(-\frac{N^2 \pi^2 c^2 \bar{\gamma}}{32 \sin^2 \theta} \right) \end{aligned} \quad (19)$$

Using (19), we can write the ASER expression of RQAM at low SNR region

$$\begin{aligned} P_{e, \text{low SNR}}^{\text{RQAM}} &= p \exp \left(-\left(\frac{\pi^2 a^2}{32} \right) N^2 \bar{\gamma} \right) + q \exp \left(-\left(\frac{\pi^2 b^2}{32} \right) N^2 \bar{\gamma} \right) \\ &\quad - \frac{2pq}{\pi} \left[\arctan \left(\frac{b}{a} \right) \exp \left(-\left(\frac{\pi^2 (a^2 + b^2)}{32} \right) N^2 \bar{\gamma} \right) \right. \\ &\quad \left. + \operatorname{arccot} \left(\frac{b}{a} \right) \exp \left(-\left(\frac{\pi^2 (a^2 + b^2)}{32} \right) N^2 \bar{\gamma} \right) \right]. \end{aligned} \quad (20)$$

Therefore, using (20) we can also state that

$$P_{e, \text{low SNR}}^{\text{RQAM}} \propto \eta_1 \exp(-\eta_2 N^2 \bar{\gamma}) \quad (21)$$

where η_1 and η_2 depend on modulation order M . Similarly, we can also obtain the ASER expression of XQAM at low SNR region.

D. High SNR Analysis for IRS

At high SNR region, one can approximate MGF expression in (3) as given below

$$\mathcal{G}_\gamma^H(s) \approx \left(\frac{\Delta_1}{s \bar{\gamma}} \right)^{0.5} \exp(-\Delta_2). \quad (22)$$

Hence, the ASER expression of RQAM at high SNR region can be expressed as

$$P_{e, \text{high SNR}}^{\text{RQAM}} = 2p \mathcal{I}^H(a, \pi/2) + 2q \mathcal{I}^H(b, \pi/2) - 2pq \left[\mathcal{I}^H(b, \arctan(b/a)) + \mathcal{I}^H(a, \operatorname{arccot}(b/a)) \right], \quad (23)$$

where the integral $\mathcal{I}^H(\cdot, \cdot)$ is given as

$$\mathcal{I}^H(c, \theta) = \frac{1}{\pi} \int_0^\theta \mathcal{G}_\gamma^H \left(\frac{c^2}{2 \sin^2 \phi} \right) d\phi, \quad (24)$$

In order to obtain insights, a closed-form solution of (24) is needed, which is given in Appendix B. Using (35), (36), and (37), we can write the ASER expression of RQAM at high SNR region

$$\begin{aligned} P_{e, \text{high SNR}}^{\text{RQAM}} &= \frac{2p \sqrt{2\Delta_1} \exp(-\Delta_2)}{\pi a \sqrt{\bar{\gamma}}} + \frac{2q \sqrt{2\Delta_1} \exp(-\Delta_2)}{\pi b \sqrt{\bar{\gamma}}} - 2pq \left[\frac{\sqrt{2\Delta_1} \exp(-\Delta_2)}{\pi b \sqrt{\bar{\gamma}}} \left(1 - \frac{a}{\sqrt{2}b} \right) \right. \\ &\quad \left. + \frac{\sqrt{2\Delta_1} \exp(-\Delta_2)}{\pi a \sqrt{\bar{\gamma}}} \left(1 - \frac{a}{\sqrt{a^2 + b^2}} \right) \right]. \end{aligned} \quad (25)$$

Therefore, using (25) we can also state that

$$P_{e,\text{low SNR}}^{\text{RQAM}} \propto \mu \sqrt{\frac{\Delta_1}{\bar{\gamma}}} \exp(-\Delta_2), \quad (26)$$

where μ depends on modulation order M . Similarly, we can also obtain the ASER expression of XQAM at low SNR region. Likewise, one can also write the ASER expression of XQAM at high SNR region.

E. Upper Bound of ASER of QAM in AWGN Channel

We can obtain upper bound of $Q_z(x, \theta)$, i.e.,

$$\begin{aligned} Q_z(x, \theta) &= \frac{1}{\pi} \int_0^\theta \exp\left(-\frac{x^2}{2 \sin^2 \phi}\right) d\phi \\ &\leq \frac{\theta}{\pi} \exp\left(-\frac{x^2}{2 \sin^2 \theta}\right) \end{aligned} \quad (27)$$

Using (27), we can get the upper bound ASER expression of RQAM in AWGN channel [21]

$$\begin{aligned} P_e^{\text{RQAM}} &\leq p \exp\left(-\frac{a^2 \bar{\gamma}}{2}\right) + q \exp\left(-\frac{b^2 \bar{\gamma}}{2}\right) - \frac{2pq}{\pi} \left[\arctan\left(\frac{b}{a}\right) + \operatorname{arccot}\left(\frac{b}{a}\right) \right] \\ &\quad \times \exp\left(-\frac{(a^2 + b^2) \bar{\gamma}}{2}\right). \end{aligned} \quad (28)$$

Using (28), we can state that

$$P_e^{\text{RQAM}} \propto \kappa_1 \exp(-\kappa_2 \bar{\gamma}). \quad (29)$$

where κ_1 and κ_2 depend on modulation order M . Using $\exp(-x) \approx 1 - x$ for small values of x , we can obtain

$$P_{e,\text{low SNR}}^{\text{RQAM}} \propto \kappa_1 (1 - \kappa_2 \bar{\gamma}). \quad (30)$$

IV. NUMERICAL RESULTS AND DISCUSSION

We present numerical results of the ASER for various QAM signaling. We plot the performance curves of the ASER P_e versus the SNR, $\bar{\gamma}$ (in dB). Simulation results are compared with numerical results for verification.

Fig. 2 depicts ASER performance of 4×2 -QAM for both AWGN and IRS-assisted wireless communications. It can be observed from Fig. 2 that an IRS-assisted scheme perform better in terms of ASER compared with an AWGN channel on low SNR regime. This is due to the fact that ASER, P_e for IRS-assisted scheme at low SNR is proportional to $\eta_1 \exp(-\eta_2 N^2 \bar{\gamma})$, while, ASER, P_e for AWGN at low SNR is proportional to $\kappa_1 (1 - \kappa_1 \bar{\gamma})$. On the other hand, ASER, P_e for IRS-assisted scheme at high SNR is slowly-decaying in comparison to AWGN scheme. This is due to the fact that ASER, P_e for IRS-assisted scheme at high SNR is proportional to $\mu \exp(-N) / \sqrt{N \bar{\gamma}}$, while, ASER, P_e for AWGN at high SNR is proportional to $\kappa_1 \exp(-\kappa_1 \bar{\gamma})$. Further, IRS-assisted system can achieve small probability of error even very low SNR region (below 0 dB) using medium and large values of N , which can be used for various low powered IoT applications.

In Fig. 3, we plot the ASER curves of an IRS-assisted scheme for different numbers of intelligent reflecting surfaces N and for 4×2 -QAM signaling. Fig.3 verifies that our analytical approximation in (3) that is based on the central limit theorem is sufficiently accurate for large values of N . For smaller values of N ($N = 4, 8, 16$), both analytical and simulation results do not match at high SNR region due to poor accuracy of approximation. However, for medium ($N = 32, 63$) and large $N = 128, 256$ values of N , both simulation and analytical results are matched closely for the whole SNR region.

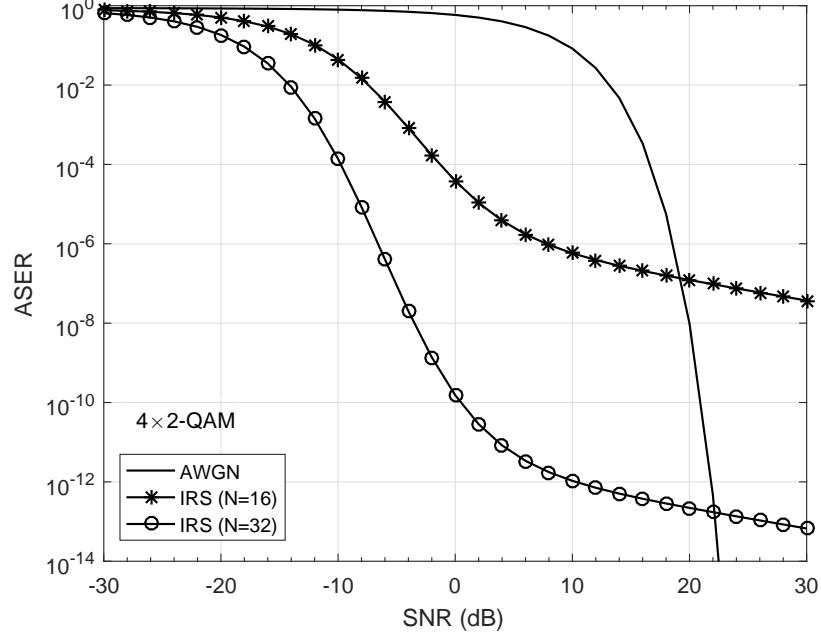


Fig. 2: ASER performance comparison of IRS-based scheme for $N = 16$ and $N = 32$ and AWGN with 4×2 -QAM.

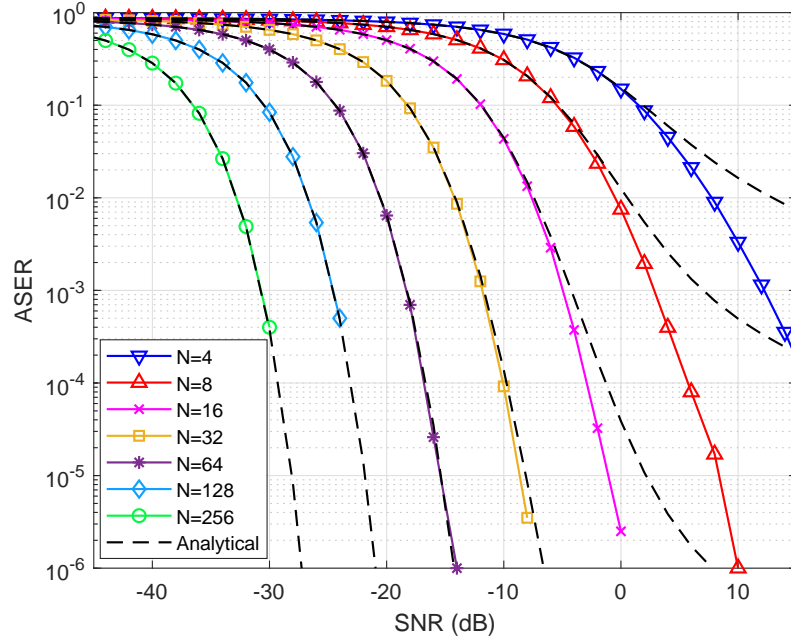


Fig. 3: ASER performance of IRS-assisted scheme for 4×2 -QAM signaling with varying N .

Fig. 4 shows the impact of N and β on ASER for two different constellations of a 32-QAM scheme such as 8×4 and 16×2 . We have chosen only two values of β ($\beta = 1$ and $\beta = 8$) for clarity in the figure. It turns out that the ASER performance improves with an increase in N , as expected. For a fixed N , the ASER performance can be controlled by the modulation parameter β . For 8×4 -QAM, a minimum ASER achieves for $\beta = 1$, for any value of N . Another observation, with increase in β , ASER

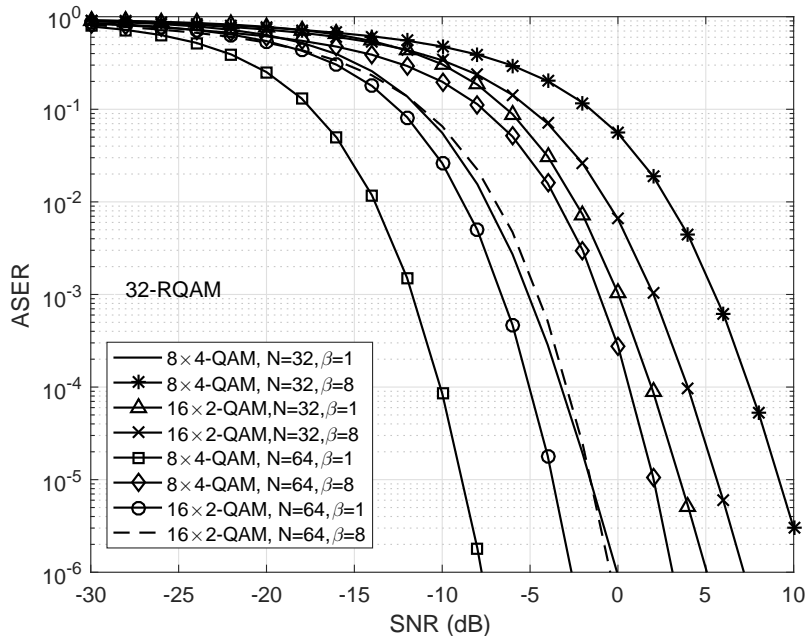


Fig. 4: ASER performance of IRS- assisted scheme for 8×4 and 16×2 constellations with varying N and β .

for the 8×4 constellation degrades fast in comparison 16×2 constellation. This can be explained from the relation among M_I , M_Q , and β . Considering a range of values of M_I , M_Q , and β , we observed that the ASER of a QAM for a fixed size (i.e., M) may vary with different constellations. For a fixed β , the ASER can be controlled by $|M_I - M_Q|$; constellation with a large $|M_I - M_Q|$ causes poor ASER relative to the constellations with a small difference. It is understood with the definition of β such as more number of constellation points in a quadrant brings them closer resulting in poor ASER. Further, for a QAM of for a fixed M , a constellation with smallest $|M_I - M_Q|$ and $\beta = 1$ is better than other constellation arrangements as it achieves a minimum ASER. In 32-QAM, the 8×4 constellation with $\beta = 1$ outperforms the 16×2 constellation with any β . Fig. 5 includes ASER curves of 8×4 -QAM with $\beta \leq 1$ for illustration and comparison.

Fig. 6 shows the impact of modulation order M on ASER performance of IRS-based wireless communications. In comparison, we have chosen 7 different RQAM from $M = 2$ to $M = 256$. It can be noticed from Fig. 6 that for a fixed ASER, the increase in M requires high SNR, as expected. Fig. 7 illustrates the comparison between RQAM and XQAM with varying N . For the purpose of comparing we have chosen 32-RQAM (8×4 , and $\beta = 1$) and 32-XQAM. It can be observed that XQAM achieves SNR gain over RQAM for a given ASER. Further, the high SNR gain can be achieved by increasing the value of N . However, the SNR gain between XQAM and RQAM for a given ASER does not change by varying N .

V. CONCLUSION

We studied the ASER performance of IRS-based radio communications over Rayleigh fading channels. New closed-form expressions of ASER for generic SNR, low SNR and high SNR regions for the considered system employing different types of QAMs signaling were obtained. The obtained analytic expressions were used to analyze the impact of different modulation parameters: M and β , and the number of IRS elements, N on the system performance. It was observed that an IRS-assisted scheme outperforms AWGN scheme on low SNR regime. This is due to the fact that ASER, P_e for IRS-assisted scheme at low SNR is proportional to $\eta_1 \exp(-\eta_2 N^2 \bar{\gamma})$, while, ASER, P_e for AWGN at low SNR is proportional to $\kappa_1 (1 - \kappa_1 \bar{\gamma})$.

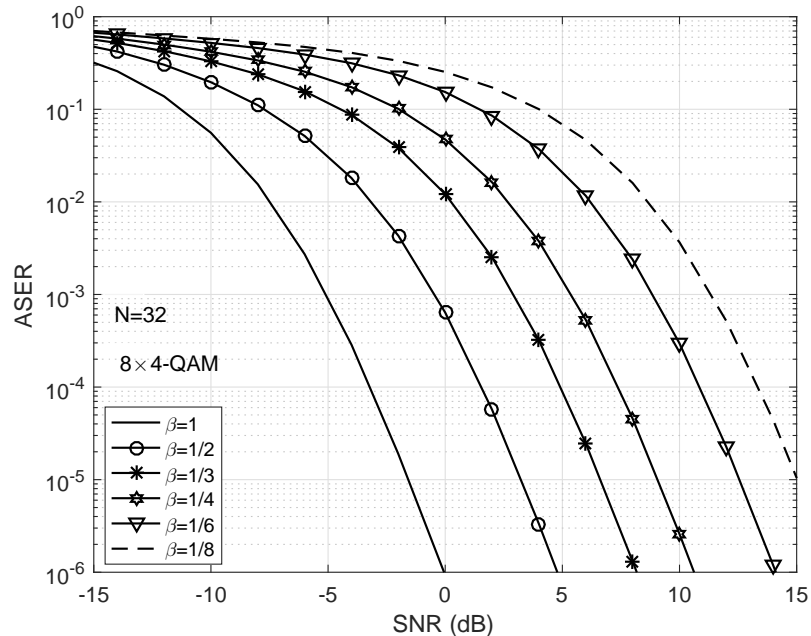


Fig. 5: ASER performance of IRS- assisted scheme for 32-RQAM (8×4) signaling with $\beta \leq 1$.

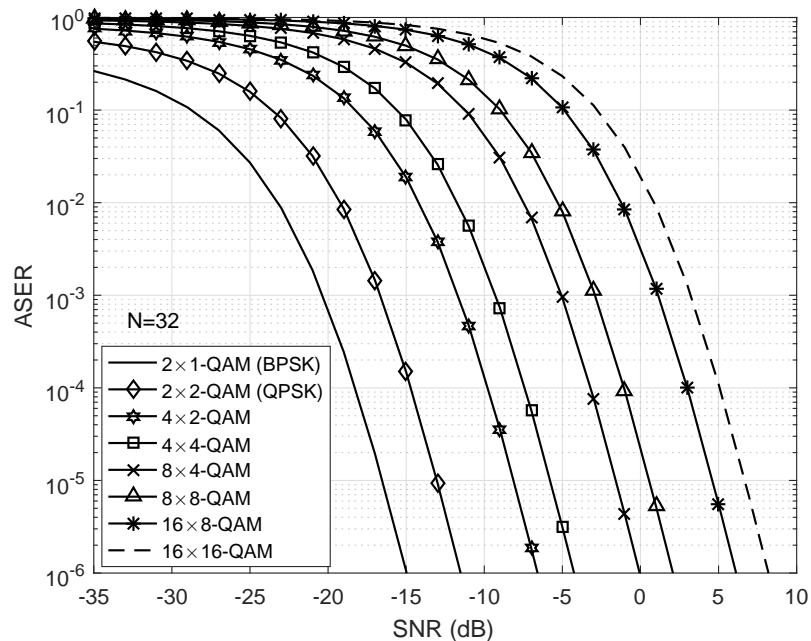


Fig. 6: Comparison of ASER performance of various RQAM for fixed $N = 32$.

While, ASER, P_e for IRS-assisted scheme at high SNR is slowly-decaying in comparison to AWGN scheme. This is due to the fact that ASER, P_e for IRS-assisted scheme at high SNR is proportional to $\mu \exp(-N) / \sqrt{N\bar{\gamma}}$, while, ASER, P_e for AWGN at high SNR is proportional to $\kappa_1 \exp(-\kappa_1 \bar{\gamma})$.

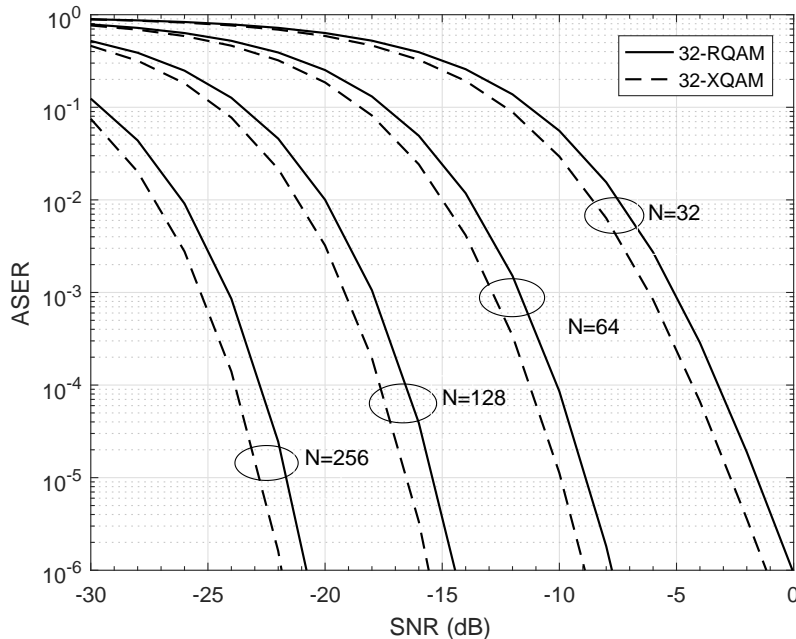


Fig. 7: Comparison of ASER performance of 32-RQAM and 32-XQAM for varying N .

APPENDIX A SOLUTION OF $\mathcal{I}(x, \theta)$

The closed-form solutions for $\mathcal{I}(x, \theta)$ are derived in terms of the confluent Lauricella's hypergeometric function, which is defined as [23, 24]

$$\begin{aligned} \Phi_1^{(n)}(m; p_1, p_2 \dots p_{n-1}; q; z_1, z_2, \dots z_n) &= \frac{\Gamma(q)}{\Gamma(m)\Gamma(q-m)} \int_0^1 v^{m-1} (1-v)^{q-m-1} \\ &\times \prod_{i=1}^{n-1} (1-vz_i)^{-p_i} \exp(vz_n) dv, \end{aligned} \quad (31)$$

where $\Gamma(\cdot)$ denotes the Gamma function. This confluent hypergeometric function can be numerically computed with the aid of its finite integral expression.

A. Closed-form Solution of $\mathcal{I}(x, \pi/2)$

Substituting, (3) into (9) followed by $t = \frac{2\Delta_1\Delta_2 \sin^2 \phi}{2\Delta_1 \sin^2 \phi + x^2\bar{\gamma}}$ and $u = \left(\frac{2\Delta_1 + x^2\bar{\gamma}}{2\Delta_1\Delta_2}\right)t$, respectively, a closed-form solution of $\mathcal{I}(x, \pi/2)$ is derived as

$$\mathcal{I}(x, \pi/2) = \frac{x\sqrt{2\Delta_1\bar{\gamma}} \exp(-\Delta_2)}{\pi(x^2\bar{\gamma} + 2\Delta_1)} \Phi_1^{(2)} \left(1; 1; 1.5; \frac{2\Delta_1}{x^2\bar{\gamma} + 2\Delta_1}, \frac{2\Delta_1\Delta_2}{x^2\bar{\gamma} + 2\Delta_1} \right), \quad (32)$$

where $\Phi_1^{(2)}(\cdot)$ is defined in (31).

B. Closed-form Solution of $\mathcal{I}(x, \arctan(y/z))$

Substituting, (3) into (9) followed by $t = \frac{2\Delta_1\Delta_2\sin^2\phi}{2\Delta_1\sin^2\phi+x^2\bar{\gamma}}$ and $u = \left(\frac{x^2(y^2+z^2)\bar{\gamma}+2\Delta_1y^2}{2\Delta_1\Delta_2y^2}\right)t$, respectively, a new closed-form solution of $\mathcal{I}(x, \arctan(y/z))$ is derived as

$$\mathcal{I}(x, \arctan(y/z)) = \frac{xy^2\sqrt{2\Delta_1\bar{\gamma}}\exp(-\Delta_2)}{2\pi(x^2(y^2+z^2)\bar{\gamma}+2\Delta_1y^2)}\Phi_1^{(3)}\left(1; 0.5, 1; 2; \frac{(x^2\bar{\gamma}+2\Delta_1)y^2}{x^2(y^2+z^2)\bar{\gamma}+2\Delta_1y^2}, \frac{2\Delta_1y^2}{x^2(y^2+z^2)\bar{\gamma}+2\Delta_1y^2}, \frac{2\Delta_1\Delta_2y^2}{x^2(y^2+z^2)\bar{\gamma}+2\Delta_1y^2}\right), \quad (33)$$

where $\Phi_1^{(3)}(\cdot)$ is defined in (31).

C. Closed-form Solution of $\mathcal{I}(x, \operatorname{arccot}(y/x))$

Substituting, (3) into (9) followed by $t = \frac{2\Delta_1\Delta_2\sin^2\phi}{2\Delta_1\sin^2\phi+x^2\bar{\gamma}}$ and $u = \left(\frac{x^2(x^2+y^2)\bar{\gamma}+2\Delta_1x^2}{2\Delta_1\Delta_2x^2}\right)t$, respectively, a new closed-form solution of $\mathcal{I}(x, \operatorname{arccot}(y/x))$ is derived as

$$\mathcal{I}(x, \operatorname{arccot}(y/x)) = \frac{x\sqrt{2\Delta_1\bar{\gamma}}\exp(-\Delta_2)}{2\pi((x^2+y^2)\bar{\gamma}+2\Delta_1)}\Phi_1^{(3)}\left(1; 0.5, 1; 2; \frac{x^2\bar{\gamma}+2\Delta_1}{(x^2+y^2)\bar{\gamma}+2\Delta_1}, \frac{2\Delta_1}{(x^2+y^2)\bar{\gamma}+2\Delta_1}, \frac{2\Delta_1\Delta_2}{(x^2+y^2)\bar{\gamma}+2\Delta_1}\right). \quad (34)$$

APPENDIX B

SOLUTION OF $\mathcal{I}^H(x, \theta)$

A. Closed-form Solution of $\mathcal{I}^H(x, \pi/2)$

Substituting, (22) into (24), a solution of $\mathcal{I}(x, \pi/2)$ is obtained as

$$\mathcal{I}^H(x, \pi/2) = \frac{\sqrt{2\Delta_1}\exp(-\Delta_2)}{\pi x\sqrt{\bar{\gamma}}}. \quad (35)$$

B. Closed-form Solution of $\mathcal{I}^H(x, \arctan(y/z))$

Substituting, (22) into (24), a solution of $\mathcal{I}^H(x, \arctan(y/z))$ is derived as

$$\mathcal{I}(x, \arctan(y/z)) = \frac{\sqrt{2\Delta_1}\exp(-\Delta_2)}{\pi x\sqrt{\bar{\gamma}}}\left(1 - \frac{z}{\sqrt{x^2+y^2}}\right). \quad (36)$$

C. Closed-form Solution of $\mathcal{I}^H(x, \operatorname{arccot}(y/x))$

Substituting, (22) into (24), a solution of $\mathcal{I}^H(x, \operatorname{arccot}(y/x))$ is got as

$$\mathcal{I}^H(x, \operatorname{arccot}(y/x)) = \frac{\sqrt{2\Delta_1}\exp(-\Delta_2)}{\pi x\sqrt{\bar{\gamma}}}\left(1 - \frac{x}{\sqrt{x^2+y^2}}\right). \quad (37)$$

REFERENCES

- [1] J. G. Andrews, S. Buzzi, W. Choi, S. V. Hanly, A. Lozano, A. C. Soong, and J. C. Zhang, "What will 5G be?" *IEEE Journal on Selected Areas in Communications*, vol. 32, no. 6, pp. 1065–1082, 2014.
- [2] Q. Wu and R. Zhang, "Towards smart and reconfigurable environment: Intelligent reflecting surface aided wireless network," *IEEE Communications Magazine*, vol. 58, no. 1, pp. 106–112, 2019.

- [3] C. Liaskos, S. Nie, A. Tsioliariidou, A. Pitsillides, S. Ioannidis, and I. Akyildiz, “A new wireless communication paradigm through software-controlled metasurfaces,” *IEEE Communications Magazine*, vol. 56, no. 9, pp. 162–169, 2018.
- [4] M. Di Renzo, M. Debbah, D.-T. Phan-Huy, A. Zappone, M.-S. Alouini, C. Yuen, V. Sciancalepore, G. C. Alexandropoulos, J. Hoydis, H. Gacanin *et al.*, “Smart radio environments empowered by reconfigurable ai meta-surfaces: an idea whose time has come,” *EURASIP Journal on Wireless Communications and Networking*, vol. 2019, no. 1, p. 129, 2019.
- [5] E. Basar, “Transmission through large intelligent surfaces: A new frontier in wireless communications,” in *2019 European Conference on Networks and Communications (EuCNC)*. IEEE, 2019, pp. 112–117.
- [6] E. C. Strinati, S. Barbarossa, J. L. Gonzalez-Jimenez, D. Ktenas, N. Cassiau, L. Maret, and C. Dehos, “6G: The next frontier: From holographic messaging to artificial intelligence using subterahertz and visible light communication,” *IEEE Vehicular Technology Magazine*, vol. 14, no. 3, pp. 42–50, 2019.
- [7] K. David and H. Berndt, “6G vision and requirements: Is there any need for beyond 5G?” *IEEE Vehicular Technology Magazine*, vol. 13, no. 3, pp. 72–80, 2018.
- [8] C. Huang, A. Zappone, G. C. Alexandropoulos, M. Debbah, and C. Yuen, “Reconfigurable intelligent surfaces for energy efficiency in wireless communication,” *IEEE Transactions on Wireless Communications*, vol. 18, no. 8, pp. 4157–4170, 2019.
- [9] Q. Wu and R. Zhang, “Intelligent reflecting surface enhanced wireless network: Joint active and passive beamforming design,” in *2018 IEEE Global Communications Conference (GLOBECOM)*. IEEE, 2018, pp. 1–6.
- [10] —, “Intelligent reflecting surface enhanced wireless network via joint active and passive beamforming,” *IEEE Transactions on Wireless Communications*, vol. 18, no. 11, pp. 5394–5409, 2019.
- [11] S. W. Ellingson, “Path loss in reconfigurable intelligent surface-enabled channels,” *arXiv preprint arXiv:1912.06759*, 2019.
- [12] A. Zappone, M. Di Renzo, F. Shams, X. Qian, and M. Debbah, “Overhead-aware design of reconfigurable intelligent surfaces in smart radio environments,” *arXiv preprint arXiv:2003.02538*, 2020.
- [13] E. Basar, M. Di Renzo, J. De Rosny, M. Debbah, M. Alouini, and R. Zhang, “Wireless communications through reconfigurable intelligent surfaces,” *IEEE Access*, vol. 7, pp. 116 753–116 773, 2019.
- [14] M. Di Renzo and J. Song, “Reflection probability in wireless networks with metasurface-coated environmental objects: an approach based on random spatial processes,” *EURASIP Journal on Wireless Communications and Networking*, vol. 2019, no. 1, p. 99, 2019.
- [15] M. A. Kishk and M.-S. Alouini, “Exploiting randomly-located blockages for large-scale deployment of intelligent surfaces,” *arXiv preprint arXiv:2001.10766*, 2020.
- [16] M. Di Renzo, F. H. Danufane, X. Xi, J. de Rosny, and S. Tretyakov, “Analytical modeling of the path-loss for reconfigurable intelligent surfaces—anomalous mirror or scatterer?” *arXiv preprint arXiv:2001.10862*, 2020.
- [17] E. Björnson, Ö. Özdogan, and E. G. Larsson, “Intelligent reflecting surface versus decode-and-forward: How large surfaces are needed to beat relaying?” *IEEE Wireless Communications Letters*, vol. 9, no. 2, pp. 244–248, 2019.
- [18] E. Björnson and L. Sanguinetti, “Power scaling laws and near-field behaviors of massive MIMO and intelligent reflecting surfaces,” *arXiv preprint arXiv:2002.04960*, 2020.
- [19] J. G. Proakis, *Digital Communications*, 4th ed. New York: McGraw-Hill, 2001.
- [20] M. K. Simon and M.-S. Alouini, *Digital Communication over Fading Channels*, 2nd ed. New York, NY, USA: Wiley, 2005.
- [21] N. C. Beaulieu, “A useful integral for wireless communication theory and its application to rectangular signaling constellation error rates,” *IEEE Transactions on Communications*, vol. 54, no. 5, pp. 802–805, May 2006.

- [22] H. Yu, G. Wei, F. Ji, and X. Zhang, “On the error probability of cross-QAM with MRC reception over generalized η - μ fading channels,” *IEEE Transactions on Vehicular Technology*, vol. 60, no. 6, pp. 2631–2643, Jul. 2011.
- [23] H. Exton, *Multiple Hypergeometric Functions and Applications*. New York: Wiley, 1976.
- [24] F. J. Lopez-Martinez, R. F. Pawula, E. Martos-Naya, and J. F. Paris, “A clarification of the proper-integral form for the Gaussian Q -function and some new results involving the F -function,” *IEEE Communications Letters*, vol. 18, no. 9, pp. 1495–1498, Sep. 2014.